ROYAL SOCIETY OF CHEMISTRY

PAPER

Check for updates

Synthesis of some new pyrimidine-based pyrene/benzochromene hybrids as EGFR kinase inhibitors in HCT-116 cancer cells through apoptosis

Yassin Adam A. Mohammed, [ID] [a] Nabila A. Kheder, [ID] [a] Mohamed S. Nafie, [ID] [bcd] Ashraf A. Abbas [ID] [a] and Kamal M. Dawood [ID] *[a]

A series of new pyrimidine-pyrene hybrids 4, naphtho[1,2-*g*][1,3,5]oxadiazocine 11 (**15**), and benzo[5,6]chromeno[4,3-*d*]pyrimidin-5-one 12 (**16**) were synthesized *via* a multicomponent one-pot Biginelli-like synthetic protocol. All the new structures were elucidated using elemental and spectroscopic techniques (^{1}H- and ^{13}C-NMR, HRMS, MALDI-TOF, IR). The cytotoxicity of the new compounds was evaluated against "HCT-116, HepG2, and WI-38" cell lines. Compounds **4b** and **4c** demonstrated the best inhibitory potency against HCT-116 cancer cells, where their IC_{50} values were 1.34 μM and 1.90 μM, compared to Erlotinib with an IC_{50} value of 1.32 μM. Further, compounds **4a** and **16** showed substantial cytotoxic effects on HCT-116 cancer cells, with IC_{50} values of 4.8 and 6.46 μM, respectively. Regarding the EGFR inhibition, compounds **4b** and **4c** exhibited IC_{50} values of 77.03 nM and 94.9 nM, respectively, compared to Erlotinib (IC_{50} = 72.3 nM). Compound **4b** treatment induced apoptosis in HCT-116 cancer cells by 30.2-fold, arresting the cell cycle at the G1-phase. It upregulated the apoptosis-related genes using the RT-PCR. Finally, a molecular docking study highlighted the binding interactions with key amino acids inside the EGFR binding site.

1. Introduction

Cancer is essentially a multifaceted family of diseases defined by the rampant proliferation of abnormal cells that can infiltrate their neighboring normal tissues as well as metastasize to distant organs. Morbidity and mortality cancer is among the top reasons of death worldwide, and it is projected to escalate to 35 million by 2050.[1] Despite the remarkable progress in early diagnosis and therapeutic measures, the problem of drug resistance, as well as the motivation to develop more potent and selective therapeutics, remains a significant challenge in the search for novel antitumor agents.[2]

Pyrene, a polyaromatic hydrocarbon (PAH), has unique advantages, such as hydrophobicity and aromaticity, that facilitate the interactions and cellular uptake with target biomolecules, resulting in enhanced therapeutic efficacy. Some pyrene-based heterocycles, as well as pyrene-based chalcones, have shown potential anticancer activity.[3–5] Also, pyrene-based heterocyclic derivatives demonstrated interesting applications with aggregation-induced

[a]Department of Chemistry, Faculty of Science, Cairo University, Giza 12613, Egypt. E-mail: kmdawood@sci.cu.edu.eg; Fax: (+202) 35727556; Tel: (+202) 35676602

[b]Department of Chemistry, College of Sciences, University of Sharjah, Sharjah 27272, United Arab Emirates

[c]Bioinformatics and Functional Genomics Research Group, Research Institute of Sciences and Engineering (RISE), University of Sharjah, Sharjah 27272, United Arab Emirates

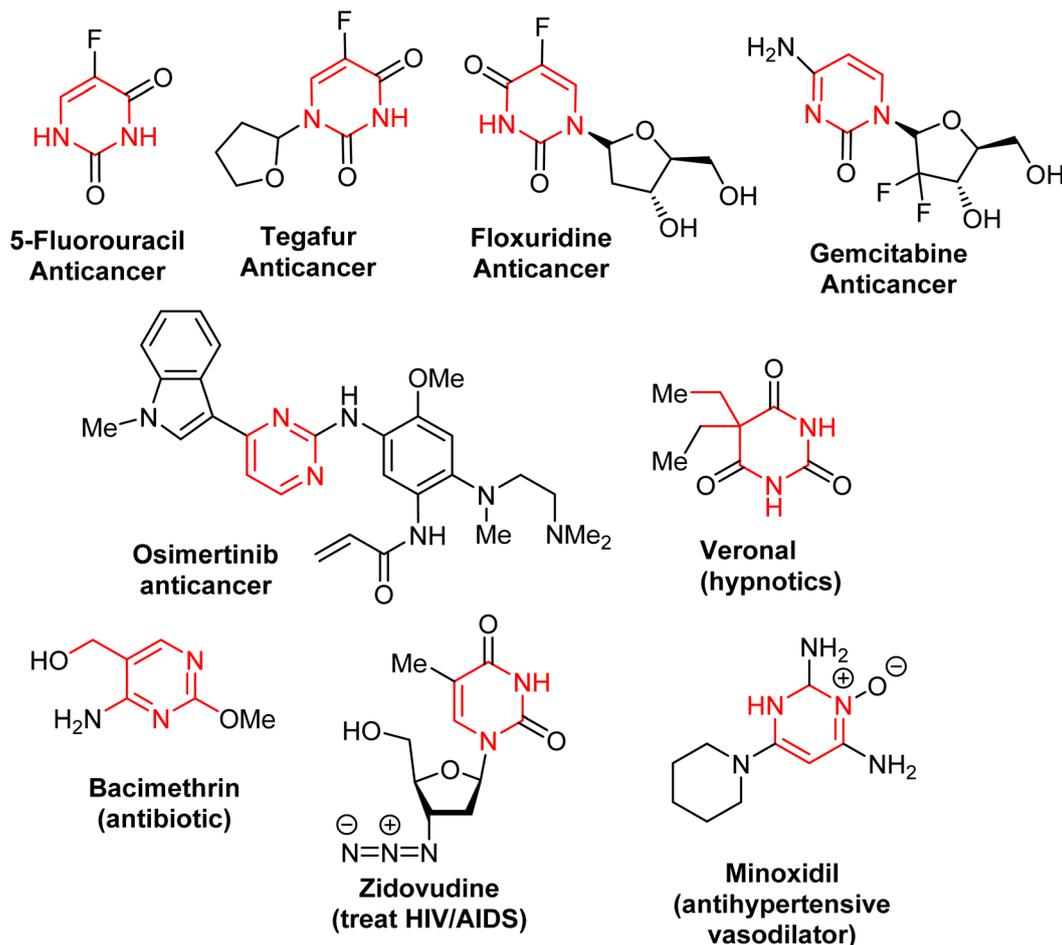*[d]Department of Chemistry, Faculty of Science, Suez Canal University, Ismailia 41522, Egypt*

emission (AIE), rendering them appropriate for imaging cancerous cells.[6–9] The pyrene-based Schiff base metal complexes were also reported to be superior anticancer therapeutics.[10–12] The pyrene-derived thiosemicarbazone metal complexes also exhibited anticancer activity toward various human cancer cells.[13–16] Pyrene derivatives have also been successfully employed in synthesizing metal–organic frameworks (MOF) and developing crystalline optoelectronic materials.[17–19] Pyrene derivatives have inhibitory effects on the migration of cancer cells, gene expression associated with metastasis (MMP-2, TGF-β), and apoptosis in both caspase-dependent and caspase-independent ways. Pyrene conjugates have also been found to overcome drug resistance by interacting with membrane-bound proteins.[20]

The pyrimidine-based organic molecules exhibit various pharmacological activities, including anticancer potency.[21] Pyrimidine-based organic molecules are the main components of some chemotherapeutic commercial drugs used to treat cancer diseases; examples of such molecules are 5-fluorouracil, tegafur, gemcitabine, floxuridine, and osimertinib (Fig. 1). Also, some other marketed FDA-approved drugs were used to treat several human diseases (Fig. 1). The Biginelli reaction is a multicomponent reaction employing 1,3-dicarbonyl substrates with aldehydes and (thio)urea to provide highly biologically active 3,4-dihydropyrimidine-2(1*H*)-one/thione adducts, particularly with anticancer activity.[22–26] Pyrimidinone derivatives have also been confirmed as potent chemotherapeutic agents, reinforcing their importance in developing new anticancer therapeutics.[27–30] Moreover, the pyrimidine derivatives were used in the

Fig. 1 Some FDA-approved drugs containing a pyrimidine moiety.

development of functional materials such as polymers,[31,32] dyes,[33] and adhesives.[34]

Benzochromene-based synthetic derivatives are an interesting class of heterocycles in the development of new pharmaceuticals against several human cancers.[35–39] The diverse therapeutic and pharmacological properties of pyrimidine, benzochromene, and pyrene scaffolds have attracted the intense interest of medicinal chemists and pharmacists. Merging two or more of these heterocyclic cores, pyrimidine-one(thione), tetra-hydropyrimidinone, benzochromene, and pyrene, offers a fertile molecular diversity ground for the design of potential anticancer agents of the future. The multiple mechanisms by which they act, such as their ability to modulate the cell cycle, induce apoptosis, and inhibit the pathways that lead to drug resistance, highlight their importance in overcoming the persistent obstacles faced in cancer treatment.

The development of effective kinase inhibitors represents a critical frontier in anticancer drug discovery. Heterocyclic scaffolds have emerged as privileged structures in medicinal chemistry, exhibiting remarkable potential as kinase inhibitors with anticancer properties.[40] Among the nitrogen heterocycles, tetrahydropyrimidine-thione, tetra-hydropyrimidinone derivatives, and pyrimidine-based derivatives are valuable pharmacophores for kinase inhibition in anticancer drug

discovery. Their structural similarity to the adenine ring of ATP allows them to mimic hinge region binding interactions in kinase active sites effectively.[41] Additionally, pyrimidines as nitrogen-containing heterocycles are isosteres of the adenine ring of ATP, enabling these molecules to mimic crucial binding interactions with kinase targets.[42] Promising pyrene-based compounds are kinase inhibitors, as they exhibit strong intercalation properties of pyrene, which contribute to their anticancer activity. When combined with established platinum-based drugs, pyrene forms robust host–guest complexes that can modulate anticancer activity with remarkable selectivity to cancer cells.[43]

Inspired by the reported anticancer activity of these scaffolds and in continuation of our research work on the synthesis and anticancer activity of a wide range of heterocycles,[44–57] herein, we have investigated a facile route to pyrene–dihydropyrimidine and benzochromene–dihydropyrimidine hybrid structures, anticipating evaluating their cytotoxic activity as well as EGFR Kinase inhibitory assay.

2. Results and discussion

2.1. Chemistry

The three-component reaction of butanamide derivatives **1a–c**, 1-pyrenecarboxaldehyde (**2**), and thiourea (**3**) under the Biginelli

© 2025 The Author(s). Published by the Royal Society of Chemistry
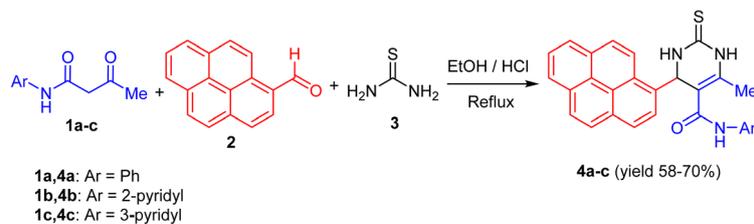
**Scheme 1** Synthesis of tetrahydropyrimidine-2-thiones **4a–c**.

condition for ten hours afforded the corresponding tetrahydro-pyrimidine-2-thione derivatives **4a–c** in 58–70% yields (Scheme 1). Elucidation of the chemical structures of the purely isolated products **4a–c** was achieved utilizing spectroscopic tools (IR, ^{1}H, and ^{13}C NMR) in addition to HRMS or MALDI-TOF spectrometry. The IR spectra of **4a–c** showed absorption bands corresponding to carbonyl function at around 1670 cm^{-1} and in the region 3150–3400 cm^{-1} for 3 NH functions. The ^{1}H-NMR spectra of **4a–c** displayed the presence of characteristic signals assigned for methyl, pyrimidine-4-CH, two NH protons of the pyrimidine ring, and the amidic proton of carboxamide function in addition to the aromatic protons at their expected values (SI files). The structures were also evidenced using ^{13}C-NMR spectral data, which revealed the presence of methyl, pyrimidine-C4, carbonyl, and thiocarbonyl carbons, as expected for these chemical skeletons (SI files).

In contrast, refluxing a mixture of the butanamide **1b**, 1-pyrenecarboxaldehyde (**2**), and urea (**5**) under typical reaction conditions did not proceed following the Biginelli pathway to provide the pyrimidine-2-one derivative **8**; however, an unexpected a mixture of the acrylamide derivatives **6** and **7** were isolated in 26% and 40% yields, respectively, as depicted in Scheme 2. An authentic sample of compound **6** was alternatively

prepared by grinding an equimolar ratio of the acetamide derivative **9** (ref. 58 and 59) with **2** in the presence of NaOH.

Next, the three-component reaction of the butanamide derivative **1a** with 2-hydroxy-1-naphthaldehyde (**10**) and thiourea (**3**) was also investigated. The reaction was completed within 10 h of reflux, giving one product as confirmed by TLC. The isolated product was established as 5-methyl-N-phenyl-3-thioxo-2,3,4,5-tetrahydro-1H-1,5-methanonaphtho[1,2-g][1,3,5]-oxadiazocine-13-carboxamide (**11a**) (86%) based on all possible analytical and spectral data, as outlined in Scheme 3.

The same three-component reaction of the butanamide derivative **1b,c** with 2-hydroxy-1-naphthaldehyde (**10**) and thiourea (**3**) was repeated under typical reaction conditions to study its scope and limitations. Thus, when compound **1c** was involved in the reaction mixture, only one product was detected
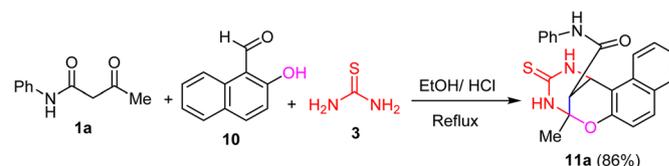
Scheme 3 Synthetic route to the polycyclic derivative **11a**.
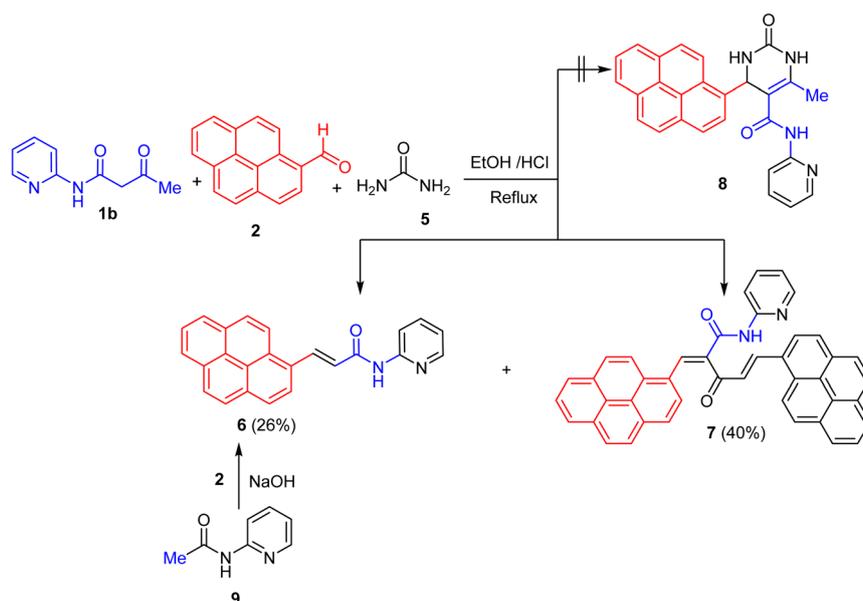
Scheme 2 An unexpected synthesis of the acrylamide derivatives **6** and **7**.
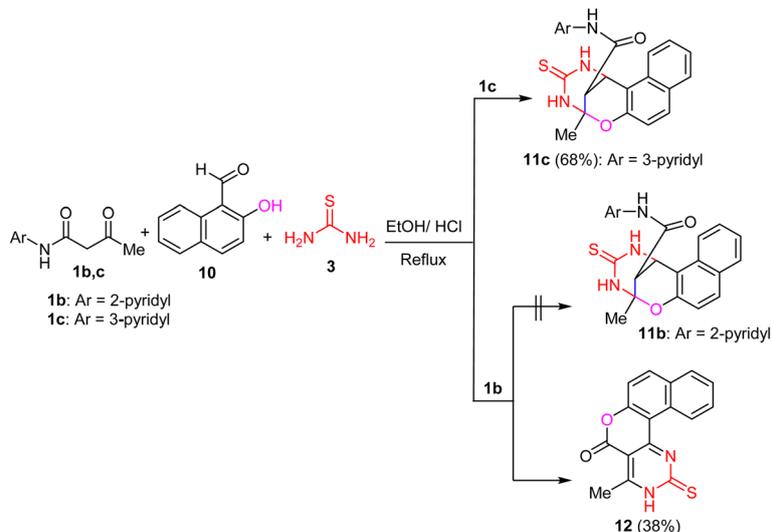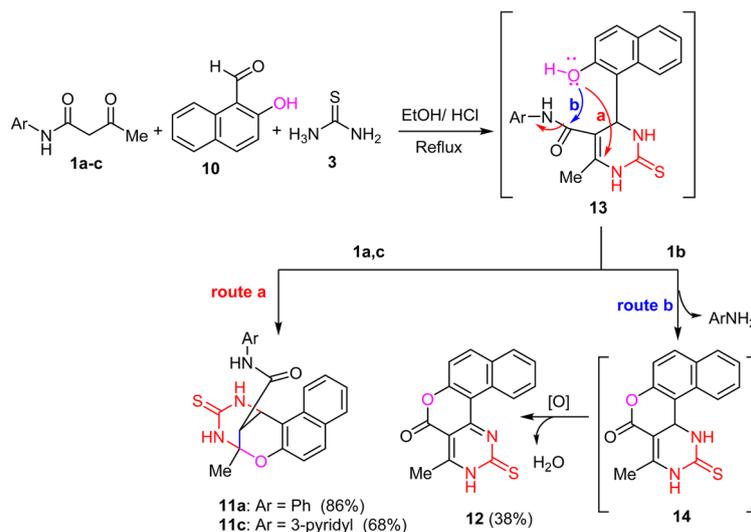
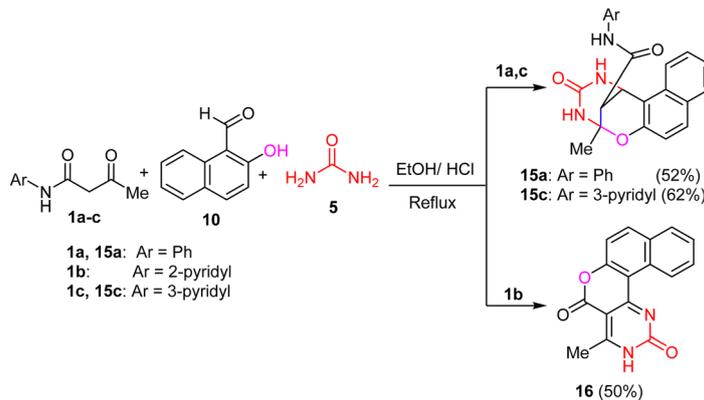**Scheme 4** The three-component reaction of **1b,c**.

by TLC, which upon purification was confirmed to be **11c** (68% yield), similar to the case of **1a**; however, when **1b** was employed instead of **1a** and **1c**, compound **12** was solely obtained (38%), but **11b** could not be detected at all (Scheme 4).

The chemical structures of the isolated products were deduced from their different analytical and spectroscopic analyses. For example, the IR of structure **11c** showed characteristic absorption bands at 3401, 3156, 3107, and 1689 cm^{-1}, corresponding to three NH and one C=O functions. The exact mass for **11c** was found to be m/z 390.020 from HRMS, which is proportionate to the calculated value of m/z 390.12. Its ^{1}H NMR displayed three characteristic singlet signals at δ 1.84, 3.28, and 5.35 due to one CH$_3$ and two CH protons in addition to the appearance of four aliphatic carbon signals in its ^{13}C NMR at δ 22.68, 43.11, 45.16, and 81.73 (for further details, see the experimental section and SI file). Also, spectral and elemental

analyses of product **12** were in complete agreement with the assigned structure. A suggested mechanism for the synthetic pathway of compounds **11a,c**, and **12** is outlined in Scheme 5.

Similarly, the reaction of butanamide derivatives **1a,c**, with 2-hydroxy-1-naphthaldehyde (**10**) and urea under similar reaction conditions gave adducts **15a,c** (Scheme 6). Compound **16** was the sole isolated product when the butanamide derivative **1b** was employed in the three-component reaction. The chemical structures of the obtained compounds were derived from their spectroscopic and analytical data. For example, the IR spectrum of compound **15a** showed characteristic absorption bands at 3427, 3299, and 3265 cm^{-1} (for three NH functions) and 1680, 1664 cm^{-1} (for two C=O functions). Its ^{1}H NMR displayed three characteristic signals at δ 1.78, 3.39, and 5.09 due to the protons of one CH$_3$ and two CH groups, in addition to the appearance of four sp^3 aliphatic carbon signals in its ^{13}C NMR

Scheme 5 A suggested synthetic route to **11a,c**, and **12**.

Scheme 6 The three-component reaction of **1a–c** with aldehyde and urea.

at δ 25.05, 43.13, 46.62, and 82.52. The chemical structures of the other isolated products **15a** and **16** were confirmed from their analytical and spectroscopic analyses as presented in the experimental section and SI files.

2.2. Biological activity

2.2.1. Cytotoxic activity. The cytotoxicity of the synthesized compounds was examined against colon (HCT-116) and liver (HepG2) cancers,[60,61] employing the 3-(4,5-dimethylthiazol-2-yl)-2,5-diphenyltetrazolium bromide salt (MTT) procedure.[60] The results are shown in Table 1 for the initial screening at a concentration of 10 μM. The IC_{50} values of compounds **4a**, **4b**, **4c**, and **16** were measured, and the results showed that the compounds were highly cytotoxic to cancer cell lines. With an inhibitory percentage of over 75% against HCT-116 cancer cells, these compounds showed a strong proportion of cell growth inhibition on the cancer cell lines, while the activity against HepG2 wasn't as promising as it was against HCT-116 cancer cells.

Calculation of the IC_{50} values of molecules **4b** and **4c** (as presented in Table 2 and Fig. 2) disclosed their potent cytotoxicity against HCT-116 cancer cells with $IC_{50} = 1.34$ μM and 1.90 μM, respectively, compared to Erlotinib ($IC_{50} = 1.32$ μM). Further, compounds **4a** and **16** showed promising cytotoxic

Table 1 Percentage of cell growth inhibition at the single dose [10 μM] for the tested compounds against HCT-116 and HepG2 cancer cell lines

Compd	Percentage of cell growth inhibition at [10 μM] ± SD	
	HCT-116	HepG2
4a	79.6 ± 2.3	26.5 ± 1.1
4b	86.3 ± 1.4	22.3 ± 1.6
4c	79.3 ± 1.9	29.8 ± 1.1
11a	68.7 ± 2.4	65.4 ± 2.3
11c	45.6 ± 1.4	46.5 ± 2.1
12	65.7 ± 2.8	34.6 ± 1.3
15a	49.3 ± 2.3	16.5 ± 0.7
15c	64.6 ± 2.2	63.5 ± 0.89
16	69.8 ± 2.1	36.5 ± 1.1
Erlotinib	88.3 ± 2.1	46.5 ± 1.3

Table 2 IC_{50} values [μM] of compounds **4a–c** and **16** against HCT-116, WI-38 cancer cells

Compd	IC_{50} [μM] ± SD^a	
	HCT-116	WI-38
4a	$4.8^b ± 0.4$	≥50
4b	1.34 ± 0.4	≥50
4c	1.90 ± 0.3	≥50
16	$6.46^b ± 0.8$	≥50
Erlotinib	1.32 ± 0.2	≥50

^{a} "IC_{50} values are expressed in Mean ± SD of three independent replicates. IC_{50} values were calculated by GraphPad Prism software". ^{b} "($P ≤ 0.05$), IC_{50} values are significantly different compared to those of Erlotinib using the unpaired t-test in GraphPad Prism".

efficacy against HCT-116 cancer cells, with IC_{50} values of 4.8 and 6.46 μM, respectively. Conversely, compounds did not exhibit cytotoxicity against normal WI-38 cells, even those with higher IC_{50} values higher than 50 μM.

The obtained cytotoxicity results of the carboxamido-pyrimidinone(thione) derivatives featuring a pyrene or benzo-chromene moiety are interesting (Tables 1 and 2) in comparison to analogous reported examples with a phenyl moiety **I** and **II** (Fig. 3).[62,63] This indicates the superiority of the current pyrene- or benzochromene-based carboxamido-pyrimidinone(thione) derivatives **4a–c** and **16**.

2.2.2. EGFR kinase inhibition. The heterocyclic derivatives **4a–c** and **16** were checked for their inhibitory activities towards the EGFR[64,65] to determine their molecular targets. The investigated molecules presented promising EGFR kinase inhibition activity (as outlined in Table 3 and Fig. 4); interestingly, compounds **4b** and **4c** exhibited $IC_{50} = 77.03$ nM and 94.9 nM, respectively, compared to Erlotinib ($IC_{50} = 72.3$ nM). Compounds **4a** exhibited potent EGFR inhibition with an $IC_{50} = 104$ nM, with an inhibition percentage of 82.3%. In comparison, **16** couldn't inhibit the EGFR with non-detected IC_{50} values.

2.2.3. Apoptosis-induction activity

2.2.3.1. Compound 4b induced apoptosis in colon cancer cells using flow cytometry. Pyrimidine-based scaffolds incorporating pyrene or benzochrome moieties exhibited potent

4b

LogIC50	0.1291
IC50	1.346
R squared	0.9934

4c

LogIC50	0.2796
IC50	1.904
R squared	0.9163

4a

LogIC50	0.6817
IC50	4.805
R squared	0.9914

16

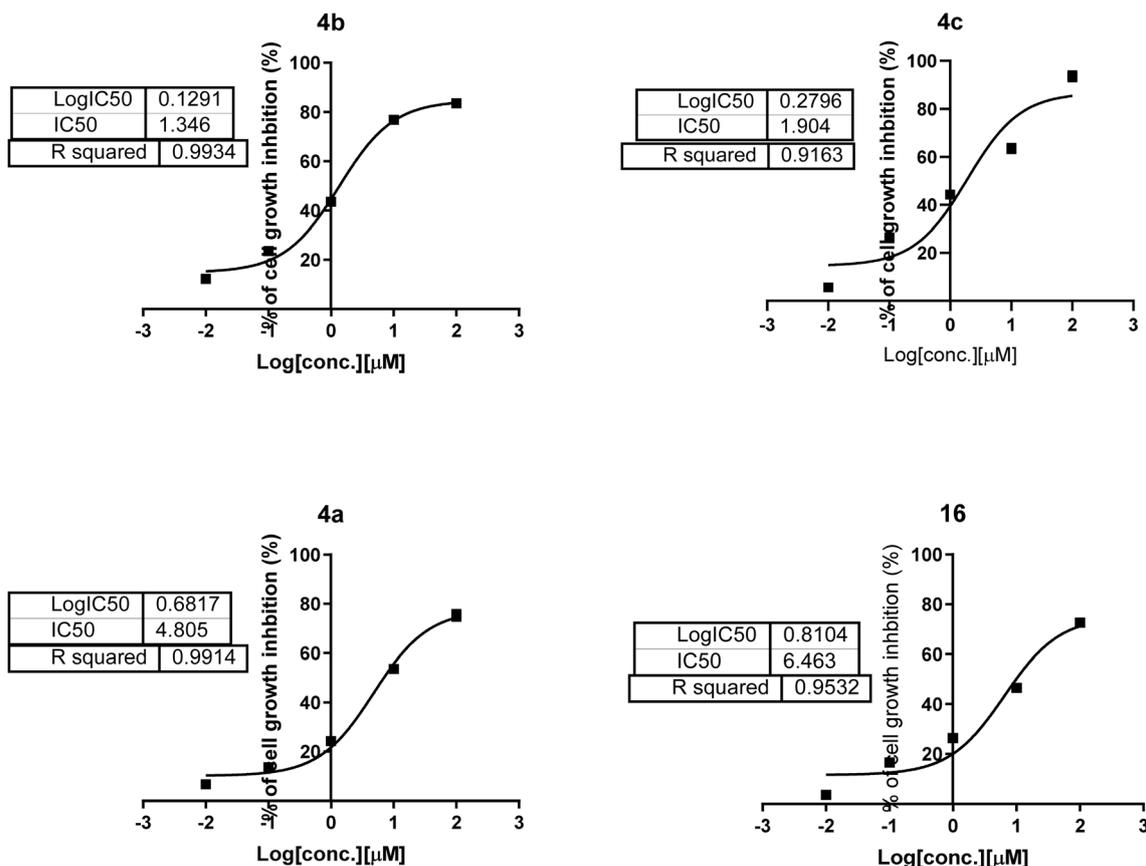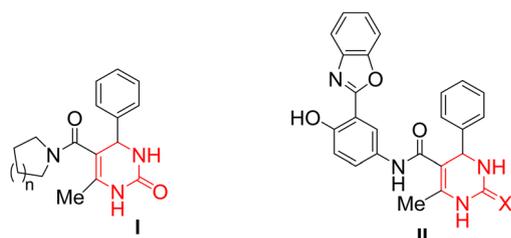| LogIC50	0.8104
IC50	6.463
R squared	0.9532

Fig. 2 Dose–response curves of the most active compounds as cytotoxic agents, highlighting IC_{50} values.

n = 1: IC_{50} = 180 μM (HepG2)
n = 2: IC_{50} = 166 μM (HepG2)

X= O: IC_{50} = > 500 μM (MCF-7)
X= S: IC_{50} = 78.5 μM (MCF-7)

Fig. 3 Reported cytotoxicity of analogous pyrimidinone(thione) derivatives I and II.

Table 3 IC_{50} values [nM] and EGFR kinases %inhibition by the most cytotoxic molecules

Compd	EGFR $IC_{50} \pm SD^{a,b}$ (nM)
4a	104 ± 5.67
4b	77.03 ± 4.36
4c	94.9 ± 4.95
16	NA
Erlotinib	72.3 ± 3.95

[a] "Values are expressed as an average of three independent replicates." "IC_{50} values were calculated using sigmoidal non-linear regression curve fit of the percentage of enzyme inhibition *versus* tested concentrations (0.001, 0.01, 0.1, 1, and 10 μM)". [b] "($P \leq 0.05$), IC_{50} values are considerably different compared to those of Erlotinib using the unpaired *t*-test in GraphPad Prism" except for **4b**.

approaches to the development of anticancer agents due to their potential to induce apoptosis specifically in cancer cells, including colon cancer.[66]

After subjecting HCT-116 cancer cells to compound **4b** (IC_{50} = 1.34 μM, 48 h), their ability to induce cell death was tested utilizing DNA-aided cell cycle analysis with cells in various stages of the cell cycle and Annexin V/PI staining. Molecule **4b** dramatically increased the percentage of colon cancer cells that died by apoptosis from 0.88% in the control group to 26.60% (19.24% early apoptosis and 7.36% late apoptosis) (as presented in Fig. 5A). In addition, 5.58% of cells died *via* necrosis, compared to 2.13% in the control.

Cell cycle analysis declared the number of cells in each phase in both treated and untreated HCT-116 cells, to disclose at which stage of the cell cycle differentiation was halted. Fig. 5B shows that compound **4b** effectively stopped cell division at the G1-phase by increasing the cell population at that stage by 87.55% compared to the control's 54.19%. The number of cells dropped throughout the S and G2/M stages.

*2.2.3.2. Compound **4b** affected apoptosis in colon cancer cells using gene expression analysis.* Among the compounds tested,
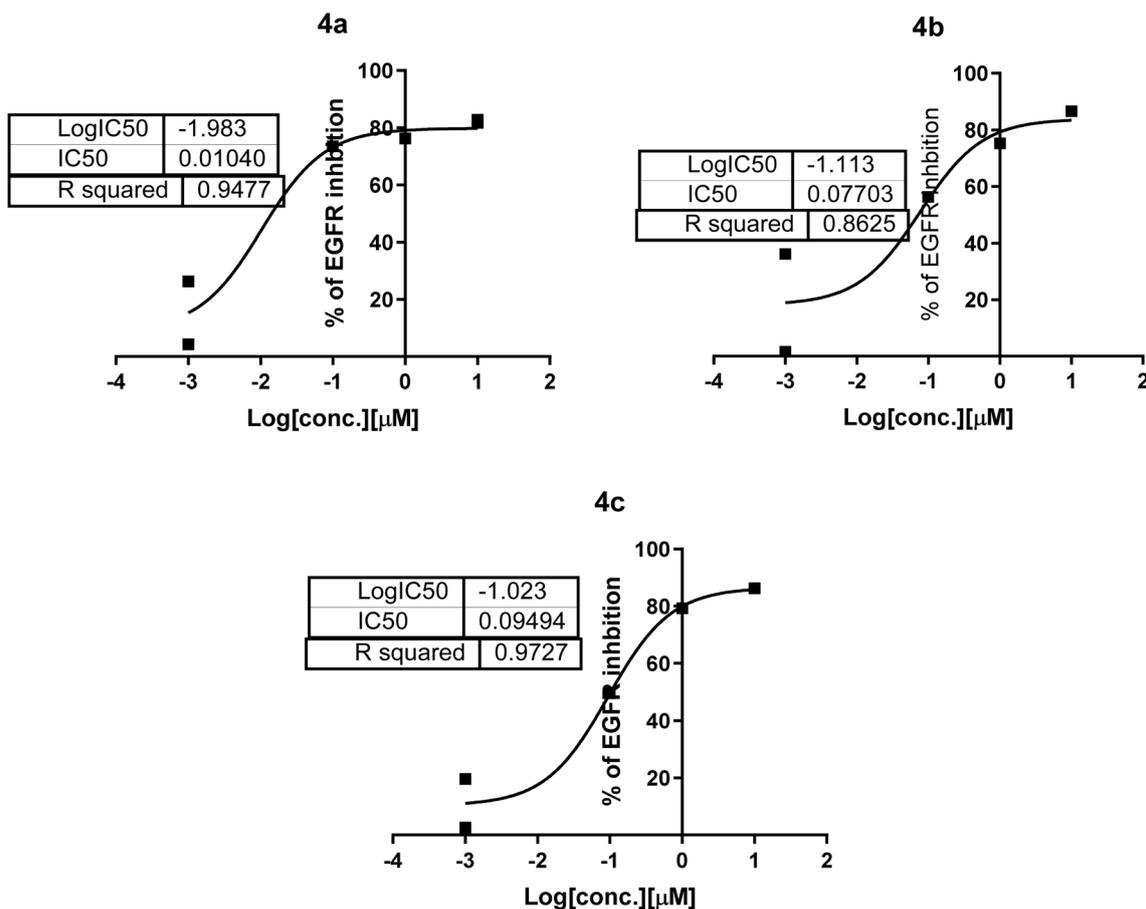
Fig. 4 Dose–response curves of the most active compounds as EGFR inhibitors, highlighting IC_{50} values from the % of EGFR inhibition *versus* the tested concentrations.

compound **4b** was the potent cytotoxic against the HCT-116 cancer cells ($IC_{50} = 1.34$ μM). Analysis of gene expression, RT-PCR, was utilized to test both the extrinsic and intrinsic genes involved in apoptotic pathways to regulate apoptosis. As shown in Fig. 6, the pro-apoptotic genes expression, including P53 (fold change = 6.85), Bax (fold change = 3.54), caspase-3 (fold change = 8.37), caspase-8 (fold change = 2.3), and caspase-9 (fold change = 6.80), was increased by compound **4b** treatment, as demonstrated in Fig. 6. In addition. The antiapoptotic gene Bcl-2 expression was simultaneously decreased by a 0.37-fold change in compound **4b** treatment. These dual pathways of compound **4b** support further development as chemotherapeutic candidates in colorectal cancer.

The findings corroborated those of the published literature,[67–70] which found that pyrene and benzochromene derivatives linked to pyrimidines promoted cell death in colon cancer cells mostly through the intrinsic mitochondrial pathway. Programmable cell death may be further enhanced by some benzochromene-containing compounds that activate the extrinsic (death receptor-mediated) pathway.

2.3. *In silico* approaches

2.3.1. Molecular docking. By blocking EGFR, colon cancer cells undergo programmed cell death, a process that has

evolved to address the specific pathophysiology of colorectal cancers. Tyrosine kinase inhibitors (TKIs) like Gefitinib or Erlotinib, as well as targeted antibodies, prevent EGFR signaling. As a result, cancer cells die off mostly *via* the intrinsic apoptotic pathway.[71]

According to the interesting EGFR inhibition potency of compound **4b**, it was screened for virtual binding towards the EGFR protein using the molecular docking approach. As shown in Table 4 and Fig. 7, compound **4b** was docked inside the EGFR binding site, maintaining the binding disposition of Erlotinib. Compound **4b** was docked inside the EGFR protein with a binding energy of -21.81 Kcal mol^{-1} and formed two H-bonds with Lys 721 (3.83 A°), and Asp 831 (1.69 A°), besides it formed the lipophilic interactions with Phe 699, Leu 694, Leu 764, Leu 820, and Pro 770. This is compared to the co-crystallized ligand (Erlotinib) that formed one H-bond interaction with Met 769 (1.36 A°). Therefore, the promising experimental inhibition of the EGFR by compound **4b** was in agreement with the docking data, which demonstrated the virtual method of binding through the pyrimidine–thione moiety for interactions towards the EGFR.

2.3.2. Physicochemical and pharmacokinetic properties. According to Lipinski's five-rule system, which includes "molecular weight, number of rotatable bonds, H-bond donors,
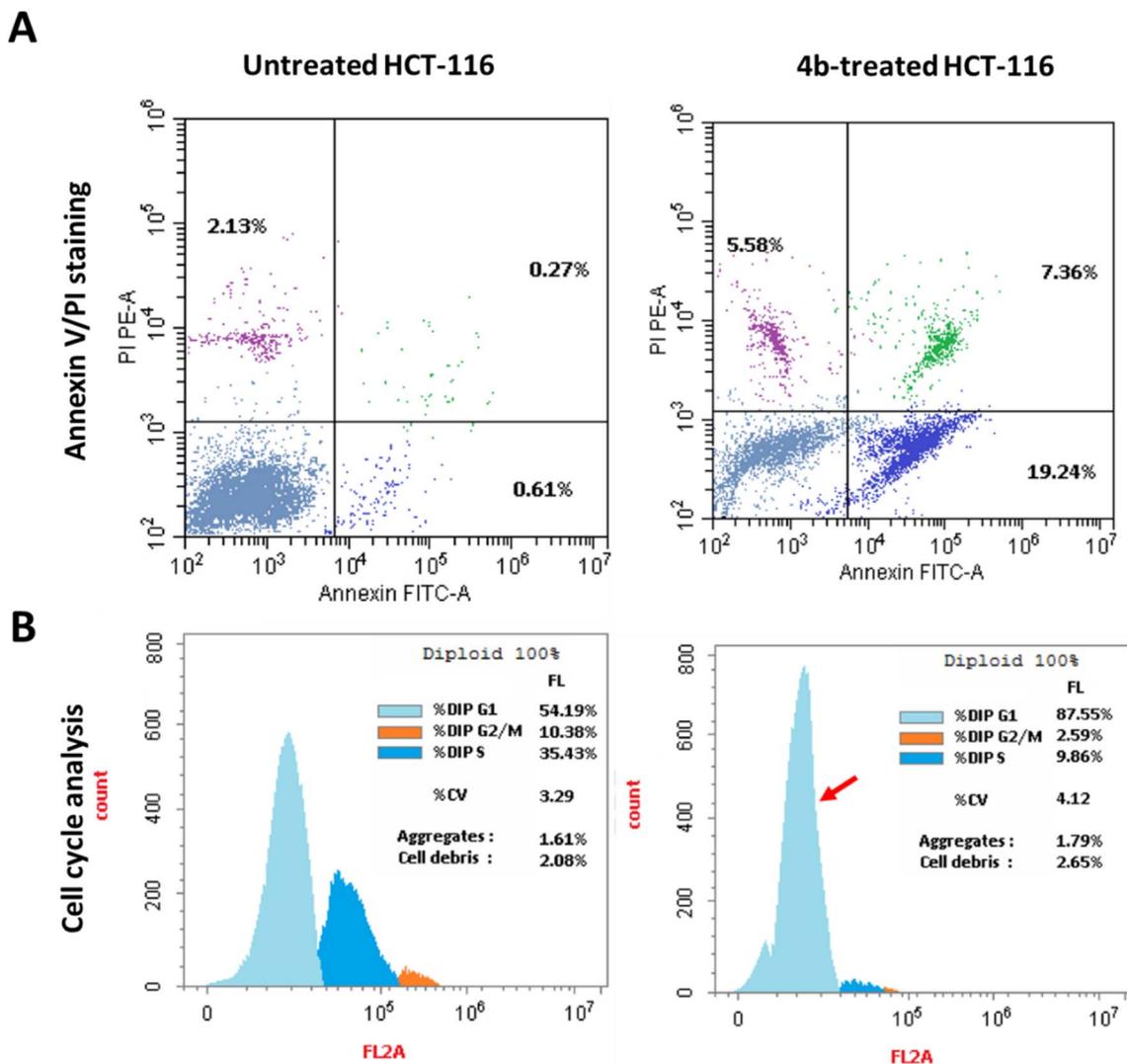
Fig. 5 Analysis of flow cytometry: upper panel (A): Annexin V/PI staining for assessment of apoptosis–necrosis, "Q1: necrosis, Q2: late apoptosis, Q4: early apoptosis". Lower panel (B): histograms of DNA content at each phase of untreated and 4b-treated HCT-116 cells with an $IC_{50} = 1.34$ μM, 48 h.
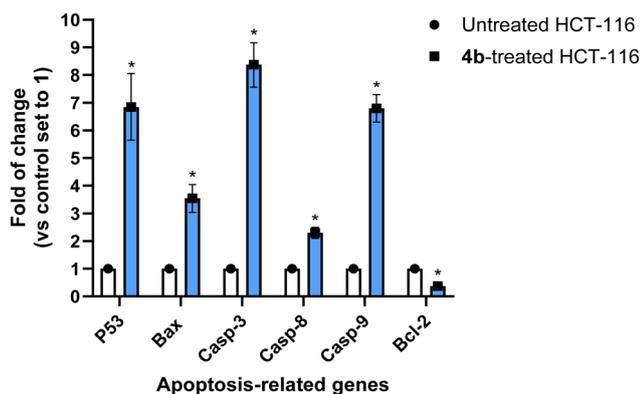

Fig. 6 The RT-PCR quantitative analysis of the apoptosis-related genes "P53, Bax, caspase-3, caspase-8, caspase-9, and Bcl-2", respectively, in untreated and treated HCT-116 cells with compound 4b ($IC_{50} = 1.34$ μM, 48 h). "*($P \leq 0.05$) is considerably varied between treated and untreated using an unpaired t-test in GraphPad Prism".

and acceptors along with a number of violations," their numbers were acceptable as shown in Table 5. The drug-likeness and physicochemical characteristics of the promising heterocyclic molecules 4a, 4b, 4c, and 16 were studied.

3. Experimental

3.1. Chemistry

3.1.1. General part. All analytical and spectroscopic tools used for the characterization of the synthesized compounds were described in the SI file.

3.1.2. Synthetic procedures

3.1.2.1. General procedure for the synthesis of tetra-hydropyrimidine derivatives 4a–c. The derivatives of the proper butanamide 1a–c (2 mmol), 1-pyrenecarboxaldehyde (0.460 g, 2 mmol), and thiourea (0.15 g, 2 mmol) were mixed and refluxed in ethyl alcohol (10 mL) using conc. hydrochloric acid (0.3 mL) as

Table 4 Interactions of ligand–receptor with binding energies (Kcal mol^{-1}) of docked molecule **4b** and Erlotinib inside the target protein of EGFR (PDB = 1M17)[a]

Molecules	Binding affinity (Kcal mol^{-1})	Type on interaction	Bond length (A°)	Amino acid
Erlotinib	−19.43	H-bond acceptor	1.36	Met 769
		It forms lipophilic interactions with Phe699, Leu 694, Leu 764, Leu 820, and Pro 770		
4b	−21.81	H-bond donor	1.69	Asp 831
		H-bond donor	3.83	Lys 721
		It forms ion-induced dipole interaction with Phe 699 and lipophilic interactions with Phe699, Leu 694, Leu 764, Leu 820, and Pro 770		

[a] Calculation of molecular docking was validated by having the RMSD value below 2.0 A° using AutoDock Vina Software.
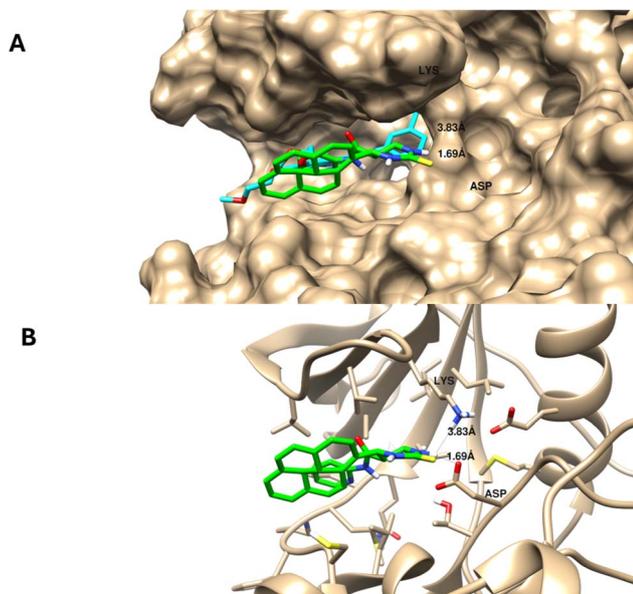

Fig. 7 Molecular docking interactions and binding disposition of the docked compound **4b** (green-colored) and the co-crystallized ligand, Erlotinib (cyan-colored). A: surface view and B: interactive view with ribbon presentation. 3D imgaes were generated by Chimera-UCSF.

a catalyst. Reflux was continued for 10 hours till a solid product was isolated. The so-formed solid products were separated by filtration, washed with ethyl alcohol, and dried under suction.

The crude products were recrystallized from EtOH/DMF to provide the respective pyrimidine-based derivatives **4a–c**.

3.1.2.1.1. 6-Methyl-N-phenyl-4-(pyren-1-yl)-2-thioxo-1,2,3,4-tetrahydropyrimidine-5-carboxamide (4a). Yellow crystals; yield 70%, m.p. >300 °C (dioxane/EtOH); IR (KBr) v 1674 (C=O), 3087 (CH aromatic), 3178, 3259, 3405 (3NH) cm^{-1}; HRMS: calcd. m/z 447.14 (M$^+$), found 447.402; ^{1}H NMR (300 MHz, DMSO-d_6) δ 2.16 (s, 3H, CH$_3$), 6.6 (s, 1H, CH), 6.92 (t, 1H, J = 9.0 Hz, ArH), 7.16 (t, 2H, J = 9.0 Hz, ArH's), 7.42 (d, 2H, J = 8.4 Hz, ArH's), 8.03–8.37 (m, 8H, ArH's), 8.57 (d, 1H, J = 9.3 Hz, ArH), 9.56 (s, 1H, NH), 9.83 (s, 1H, NH), 10.14 (s, 1H, NH); ^{13}C NMR (75 MHz, DMSO-d_6) δ 16.58, 51.80, 66.39, 108.02, 119.56, 123.12, 123.39, 123.93, 125.11, 125.52, 125.60, 125.90, 126.36, 127.14, 127.30, 127.65, 128.55, 128.68, 130.20, 130.47, 130.88, 135.03, 136.99, 138.79, 164.88, 173.96. Anal. Calcd. for C$_{28}$H$_{21}$N$_3$OS (447.56): C, 75.14; H, 4.73; N, 9.39. Found: C, 75.22; H, 4.68; N, 9.42.

3.1.2.1.2. 6-Methyl-4-(pyren-1-yl)-N-(pyridin-2-yl)-2-thioxo-1,2,3,4-tetrahydropyrimidine-5-carboxamide (4b). Brown crystals; yield 62%, m.p. 290–2 °C (DMF/EtOH); IR (KBr) v 1650 (C=O), 3009 (CH aromatic), 3203, 3421 (broad, 3NH) cm^{-1}; MS: MALDI-TOF: calcd for [M + K]$^+$ m/z = 487.10; found 487.079; ^{1}H NMR (300 MHz, DMSO-d_6) δ 2.19 (s, 3H, CH$_3$), 6.65 (d, 1H, CH, J = 2.4 Hz), 6.96 (m, 1H, ArH), 7.56 (m, 1H, ArH), 7.73 (d, 1H, J = 8.1 Hz, ArH), 8.02–8.28 (m, 8H, ArH's), 8.34 (d, 1H, J = 8.8 Hz, ArH), 8.58 (d, 1H, J = 9.3 Hz, ArH), 9.53 (s, 1H, NH), 10.13 (s, 1H, NH), 10.34 (s, 1H, NH); ^{13}C NMR (75 MHz, DMSO-d_6) δ 16.68, 51.62, 106.98, 113.89, 119.34, 123.20, 123.87, 123.89, 125.07, 125.46,

Table 5 ADME pharmacokinetics and molecular properties of the promising derivatives[a]

#	Molsoft				Molinspiration 2018.10						SwissADME
	HBA	HBD	Solubility (mg L^{-1})	Drug score	MWt (D)	MV (A^3)	PSA (A^2)	log p	BBB score	Nviolations	Drug likeness (Lipinski Pfizer filter)
4a	2	3	0.03	0.36	447.1	470.54	44.95	6.09	3.40	1 Log p > 5	Yes
4b	3	3	0.21	0.80	448.1	465.3	54.57	5.72	2.78	1 Log p > 5	Yes
4c	3	3	0.61	1.09	448.1	54.47	466.0	5.32	2.92	1 Log p > 5	Yes
16	4	1	769.79	−0.73	278.0	51.80	296.8	1.49	4.31	0	Yes

[a] "Mwt: molecular weight, MV: molecular volume, PAS: polar surface area, log p: log P: octanol–water partition coefficient, nrotb: number of rotatable bonds, nviolations: number of violations, HBA: hydrogen bond acceptor, HBD: hydrogen bond donor, drug-likeness score, compounds having negative or zero value should not be considered as drug-like". "Drug likeness (Lipinski Pfizer filter)/"Yes, drug-like" MW ≤ 500, log p ≤ 5, HBA ≤ 10 and HBD ≤ 5".

125.50, 126.21, 126.32, 127.27, 127.55, 130.18, 130.47, 130.83, 136.43, 136.64, 137.87, 147.75, 151.81, 162.34, 165.55, 173.58. Anal. Calcd. for $C_{27}H_{20}N_4OS$ (448.54): C, 72.30; H, 4.49; N, 12.49. Found: C, 72.25; H, 4.38; N, 12.53.

3.1.2.1.3. 6-Methyl-4-(pyren-1-yl)-N-(pyridin-3-yl)-2-thioxo-1,2,3,4-tetrahydropyrimidine-5-carboxamide (4c). Dark yellow crystals; yield 58%, m.p. >300 °C (Dioxane/EtOH); IR (KBr) ν 1694 (C=O), 3041 (CH aromatic), 3249–3433 (br, 3NH) cm^{-1}; MS: MALDI-TOF: calcd for [M + K]$^+$ m/z = 487.10; found 487.126; ^{1}H NMR (300 MHz, DMSO-d_6) δ 2.19 (s, 3H, CH$_3$), 6.61 (d, 1H, CH, J = 2.4 Hz), 7.18 (m, 1H, ArH), 7.82 (d, 1H, J = 9.3 Hz. ArH), 8.03–8.38 (m, 9H, ArH's), 8.58 (m, 2H, ArH's), 9.64 (s, 1H, NH), 10.06 (s, 1H, NH), 10.22 (s, 1H, NH); ^{13}C NMR (75 MHz, DMSO-d_6) δ 16.42, 51.55, 66.22, 107.24, 122.83, 123.38, 123.71, 123.74, 124.99, 125.40, 125.45, 125.66, 126.25, 126.44, 126.91, 127.14, 127.51, 129.99, 130.34, 130.70, 135.26, 135.66, 136.66, 140.83, 144.07, 165.22, 173.79. Anal. Calcd. for $C_{27}H_{20}N_4OS$ (448.54): C, 72.30; H, 4.49; N, 12.49. Found: C, 72.27; H, 4.53; N, 12.42.

3.1.2.2. Synthesis of the acrylamide derivatives 6 and 7. The butanamide derivative **1b** (0.356 g, 2 mmol), 1-pyrencarboxaldehyde (0.460 g, 2 mmol), and urea (0.12 g, 2 mmol) were mixed and refluxed in ethyl alcohol (10 mL) using conc. hydrochloric acid (0.3 mL) as a catalyst. Reflux was continued for 10 hours till a solid product was isolated. The so-formed solid products were separated by filtration, washed with ethyl alcohol, and dried under suction. Fractional recrystallization of the crude products from EtOH/DMF provided the respective acrylamides **6** and **7**.

3.1.2.2.1. (E)-3-(Pyren-1-yl)-N-(pyridin-2-yl)acrylamide (6). Brown crystals; yield 26%, m.p. 289–290 °C (DMF/EtOH); IR (KBr) ν 3426 (NH), 3036 (CH aromatic), 1679 (C=O), 1581 (C=C) cm^{-1}; ^{1}H NMR (300 MHz, DMSO-d_6) δ 7.16 (t, 1H, J = 6.0 Hz, ArH), 7.32 (d, 1H, J = 15.3 Hz, CH=), 7.86 (t, 1H, J = 6.0 Hz, ArH), 8.09–8.37 (m, 10H, ArH's), 8.58 (d, 1H, J = 9.3 Hz, ArH), 8.74 (d, 1H, J = 15.3 Hz, CH=), 10.83 (s, 1H, NH); ^{13}C NMR (75 MHz, DMSO-d_6) δ 113.84, 119.65, 122.56, 123.84, 124.17, 124.30, 124.69, 125.46, 125.89, 126.15, 126.73, 127.43, 128.45, 128.54, 128.71, 128.97, 130.30, 130.93, 131.95, 137.23, 138.35, 148.23, 152.32, 164.28. Anal. Calcd. for $C_{24}H_{16}N_2O$ (348.41): C, 82.74; H, 4.63; N, 8.04. Found: C, 82.68; H, 4.72; N, 8.12.

3.1.2.2.2. (2E,4E)-3-Oxo-5-(pyren-1-yl)-2-(pyren-1-ylmethyl-ene)-N-(pyridin-2-yl)pent-4-enamide (7). Yellow crystals; yield 40%, m.p. 292 °C (DMF); IR (KBr) ν 3435 (broad NH), 3101 (CH aromatic), 1672 (C=O), 1649 (C=O), 1578 (C=C) cm^{-1}; MS: MALDI-TOF: calcd for [M + K]$^+$ m/z = 641.16; found 641.50; ^{1}H NMR (300 MHz, DMSO-d_6) δ 7.20 (t, 1H, J = 6.0 Hz, ArH), 7.36 (d, 1H, J = 15.6 Hz, CH=), 7.46 (t, 1H, J = 6.0 Hz, ArH), 7.71 (d, 1H, J = 7.8 Hz, ArH), 7.80 (d, 1H, J = 8.7 Hz, ArH), 7.92 (t, 1H, J = 6.0 Hz, ArH), 8.09–8.52 (m, 16H, ArH's), 8.58 (d, 1H, J = 9.3 Hz, ArH), 8.76 (d, 1H, J = 15.6 Hz, CH=), 11.13 (s, 1H), 12.9 (br.s, 1H, NH); ^{13}C NMR (75 MHz, DMSO-d_6) δ 61.32, 114.16, 116.33, 119.73, 120.30, 122.24, 122.53, 123.65, 123.84, 123.91, 124.17, 124.35, 125.47, 125.73, 125.93, 126.19, 126.42, 126.74, 126.94, 127.00, 127.25, 127.43, 128.31, 128.42, 128.52, 128.75, 129.03, 129.19, 130.13, 130.29, 130.81, 130.93, 131.84, 132.04, 137.60, 139.27, 140.55, 146.72, 147.18, 149.57, 151.83, 164.56, 166.21.

Anal. Calcd. for $C_{43}H_{26}N_2O_2$ (602.68): C, 85.69; H, 4.35; N, 4.65. Found: C, 85.72; H, 4.28; N, 4.77.

3.1.2.3. Green synthesis of the acrylamide derivative 6. In a mortar, 1-pyrenecarboxaldehyde (0.46 g, 2 mmol), N-(pyridin-2-yl)acetamide (0.27 g, 2 mmol),[58,59] and NaOH (0.16 g, 4 mmol) were mixed and ground for 30 minutes. Then, the obtained mixture was added to cold water, and aqueous hydrochloric acid was added dropwise to neutralize the solution. The solid product that formed was separated by filtration and dried under suction. The crude product was recrystallized from ethanol to give a solid product identical to the acrylamide derivative **6**.

3.1.2.4. Synthesis of compounds 11a,c and 12. The derivatives of the proper butanamide **1a–c** (2 mmol), 2-hydroxy-1-naphthaldehyde (0.344 g, 2 mmol), and thiourea (0.15 g, 2 mmol) were mixed and refluxed in ethyl alcohol (10 mL) using six drops of conc. hydrochloric acid (0.3 mL) as a catalyst. Reflux was continued for 10 hours till a solid product was isolated. The so-formed solid products were separated by filtration, washed with ethyl alcohol, and dried under suction. The crude products were recrystallized from EtOH/DMF to provide the respective products outlined in Schemes 3 and 4.

3.1.2.4.1. 5-Methyl-N-phenyl-3-thioxo-2,3,4,5-tetrahydro-1H-1,5-methanonaphtho[1,2-g][1,3,5]-oxadiazocine-13-carboxamide (11a). Yellow crystals; yield 86%, m.p. >300 °C (DMF/EtOH); IR (KBr) ν 3395, 3336 (2NH), 3059 (CH aromatic), 1663 (C=O) cm^{-1}; HRMS: calcd. m/z 389.12 (M$^+$), found 389.7741; ^{1}H NMR (500 MHz, DMSO-d_6) δ 1.83 (s, 3H, CH$_3$), 3.22 (s, 1H, CH–CO), 5.30 (s, 1H, CH–NH), 7.31–8.17 (m, 11H, AH's), 9.06 (s, 1H, D$_2$O-exchangeable NH), 9.34 (s, 1H, D$_2$O-exchangeable NH), 10.17 (s, 1H, D$_2$O-exchangeable NH); ^{13}C NMR (APT) (125 MHz, DMSO-d_6) δ 23.12 (CH$_3$), 43.54 (CH), 45.73 (CH), 82.29 (C), 116.59 (C), 118.59 (CH), 119.41 (CH), 122.59 (CH), 123.93 (CH), 124.37 (CH), 127.50 (CH), 128.84 (CH), 129.05 (C), 129.31 (CH), 130.59 (CH), 131.26 (C), 139.40 (C), 148.86 (C), 166.78 (C=O), 176.97 (C=S). Anal. Calcd. For $C_{22}H_{19}N_3O_2S$ (389.47): C, 67.85; H, 4.92; N, 10.79. Found: C, 67.72; H, 4.88; N, 10.85.

3.1.2.4.2. 5-Methyl-N-(pyridin-3-yl)-3-thioxo-2,3,4,5-tetra-hydro-1H-1,5-methanonaphtho[1,2-g][1,3,5]-oxadiazocine-13-carboxamide (11c). Orange crystals; yield 68%, m.p. >300 °C (DMF/EtOH); IR (KBr) ν 3401 (NH), 3156 (NH), 3107 (NH), 3029 (CH aromatic), 2910 (CH aliphatic), 1689 (C=O), 1623 (C=N) cm^{-1}; HRMS: calcd. m/z 390.12 (M$^+$), found 390.020; ^{1}H NMR (500 MHz, DMSO-d_6) δ 1.84 (s, 3H, CH$_3$), 3.28 (s, 1H, CH–CO), 5.35 (s, 1H, CH–NH), 7.09–8.27 (m, 9H, ArH's), 8.71 (s, 1H, ArH), 9.09 (s, 1H, D$_2$O-exchangeable NH), 9.34 (s, 1H, D$_2$O-exchangeable NH), 10.42 (s, 1H, D$_2$O-exchangeable NH); ^{13}C NMR (75 MHz, DMSO-d_6) δ 22.68, 43.11, 45.16, 81.73, 115.95, 118.13, 122.07, 123.86, 124.01, 126.12, 127.14, 128.42, 128.63, 130.24, 130.74, 135.57, 140.53, 144.49, 148.36, 166.98, 176.55. Anal. Calcd. for $C_{21}H_{18}N_4O_2S$ (390.46): C, 64.60; H, 4.65; N, 14.35. Found: C, 64.52; H, 4.77; N, 14.42.

3.1.2.4.3. 4-Methyl-2-thioxo-2,3-dihydro-5H-benzo[5,6]chro-meno[4,3-d]pyrimidin-5-one (12). Red crystals; yield 38%, m.p. 220–222 °C (DMF/EtOH); IR (KBr) ν 3141 (NH), 1708 (C=O) cm^{-1}; HRMS: m/z 294.05 (M$^+$), found 294.183; ^{1}H NMR (300

MHz, DMSO-d_6) δ 2.62 (s, 3H, CH$_3$), 7.48 (d, 1H, J = 9.3 Hz, ArH's), 7.60–7.63 (m, 1H, ArH), 7.69–7.74 (m, 1H, ArH),7.99 (d, 1H, J = 7.2 Hz, ArH), 8.21 (d, 1H, J = 9.3 Hz, ArH), 8.46 (d, 1H, J = 8.1 Hz, ArH), 9.11 (s, 1H, NH); ^{13}C NMR (125 MHz, DMSO-d_6) δ 30.60, 100.01, 112.79, 116.90, 122.78, 123.44, 127.04, 129.63, 129.85, 130.34, 136.71, 142.89, 155.81, 158.92, 175. 51, 195.59. Anal. Calcd. for C$_{16}$H$_{10}$N$_2$O$_2$S (294.33): C, 65.29; H, 3.42; N, 9.52. Found: C, 65.17; H, 3.38; N, 9.66.

3.1.2.5. General procedure for the reaction with urea. The reaction of appropriate butanamide **1a–c** (2 mmol), 2-hydroxy-1-naphthaldehyde (0.344 g, 2 mmol), and urea (2 mmol) under the same experimental conditions as above afforded **15a,c** in the case of **1a** and **1c**. However, compound **16** was obtained by using **1b** as outlined in Scheme 6.

3.1.2.5.1. 5-Methyl-3-oxo-N-phenyl-2,3,4,5-tetrahydro-1H-1,5-methanonaphtho[1,2-g][1,3,5]oxadiazocine-13-carboxamide (15a). Orange crystals; yield 52%, m.p. 291–293 °C (DMF/EtOH); IR (KBr) ν 3427, 3299, 3265 (3NH), 3094 (CH aromatic), 1680, 1664 (2C=O) cm^{-1}; HRMS: calcd m/z 373.14 (M$^+$), found 373.99; ^{1}H NMR (300 MHz, DMSO-d_6) δ 1.78 (s, 3H, CH$_3$), 3.39 (d, 1H, J = 3.0 Hz, CH–CO), 5.09 (d, 1H, J = 3.0 Hz, CH–NH), 6.98–8.05 (m, 13H, ArH's + 2NH), 10.14 (s, 1H, D$_2$O-exchangeable NH); ^{13}C NMR (APT) (125 MHz, DMSO-d_6) δ 25.05 (CH$_3$), 43.13 (CH), 46.62 (CH), 82.52 (C), 116.55 (C), 118.85 (CH), 119.72 (CH), 122.41 (CH), 123.72 (CH), 123.96 (CH), 126.96 (CH), 128.74 (CH), 129.14 (C), 129.20 (CH), 129.29 (CH), 131.61 (C), 139.09 (C), 149.61 (C), 155.46 (C=O), 166.41 (C=O). Anal. Calcd. For C$_{22}$H$_{19}$N$_3$O$_3$ (373.41): C, 70.76; H, 5.13; N, 11.25. Found: C, 70.68; H, 5.22; N, 11.33.

3.1.2.5.2. 5-Methyl-3-oxo-N-(pyridin-3-yl)-2,3,4,5-tetrahydro-1H-1,5-methanonaphtho[1,2-g][1,3,5]-oxadiazocine-13-carboxamide (15c). Brown crystals; yield 62%, m.p. 292–294 °C (DMF/EtOH); IR (KBr) ν 3407 (NH), 3172 (NH), 3038 (CH aromatic), 1693, 1647 (2C=O) cm^{-1}; HRMS: calcd. m/z 374.14 (M$^+$), found 374.470 ^{1}H NMR (300 MHz, DMSO-d_6) δ 1.81 (s, 3H, CH$_3$), 3.3 (s, 1H, CH–CO), 5.24 (s, 1H, CH–NH), 7.06–8.11 (m, 10H, ArH's), 8.31 (br.s, 1H, NH), 8.76 (br.s, 1H, NH), 10.44 (s, 1H, NH); ^{13}C NMR (75 MHz, DMSO-d_6) δ 23.58, 44.55, 44.84, 83.59, 117.44, 118.61, 122.08, 123.80, 126.19, 126.99, 128.49, 128.61, 129.29, 129.91, 130.96, 140.59, 144.40, 148.51, 154.80, 167.79. Anal. Calcd. for C$_{21}$H$_{18}$N$_4$O$_3$ (374.40): C, 67.37; H, 4.85; N, 14.96. Found: C, 67.42; H, 4.77; N, 14.82.

3.1.2.5.3. 4-Methyl-2H-benzo[5,6]chromeno[4,3-d]pyrimidine-2,5(3H)-dione (16). Yellow crystals; yield 50%, m.p.269–271 °C (DMF/EtOH); IR (KBr) ν 3429 (NH), 1711, 1655 (2C=O) cm^{-1}; ^{1}H NMR (500 MHz, DMSO-d_6) δ 2.62 (s, 3H, CH$_3$), 7.57–8.58 (m, 6H, ArH's), 9.23 (s, 1H, NH); ^{13}C NMR (DMSO-d_6) δ 30.36, 99.99, 112.85, 116.95, 122.84, 123.54, 127.05, 127.39, 129.63, 129.88, 130.39, 136.72, 142.93, 155.86, 158.95, 195.61. Anal. Calcd. for C$_{16}$H$_{10}$N$_2$O$_3$ (278.27): C, 69.06; H, 3.62; N, 10.07. Found: C, 69.13; H, 3.51; N, 10.15.

3.2. Anticancer evaluation

The biological activities of compounds were partially performed at "Center of Excellence in molecular medicine", Suez Canal University, including cytotoxicity against tested cell lines, and EGFR target inhibition. Annexin V/PI with cell cycle analysis compound **4b** was performed at the confirmatory diagnostic unit VACSERA-EGYPT. Colon (HCT-116), liver (HepG2) cancer cells, and normal WI-38 cell lines were purchased from the National Cancer Institute, Cairo, Egypt.

3.2.1. Cytotoxicity using MTT assay. The percentage of cell growth inhibition at the single dose [10 μM] and cytotoxicity (IC$_{50}$) were determined using the MTT assay,[60] against HCT-116, HepG2, and WI-38 cell lines. This was carried out preliminary to determine a single dose % inhibition at 10 μM for the compounds to select the most cytotoxic ones among them as anticancer agents. Then, the cytotoxicity of the drugs on the cancer cell line compared to the normal cell line was evaluated. Cells were treated for 48 h with different concentrations "0.01, 0.1, 1, 10, and 100 μM" of the selected compounds. The optical density (O.D.) was measured spectrophotometrically at 570 nm using an ELISA microplate reader (Sunrise TM, TECAN, Germany). Following the previous literature,[60,61] the mean values were calculated as the percentage of cell viability as follows:

$$\% \text{ Cell viability} = \frac{\text{OD(treated cells)}}{\text{OD(control cells)}} \times 100$$

3.2.2. EGFR kinase inhibitory assay. Compounds **4a**, **4b**, **4c** and **16** were evaluated for the EGFR kinase inhibition "Catalog #40321". They were dissolved in DMSO (0.1%), and four serial concentrations of "0.001, 0.01, 0.1, 1, and 10 μM" were prepared following the manufacturer's instructions.[62,63]

3.2.3. Annexin V/PI staining and cell cycle analysis. The HCT-116 cells were treated with the pyrimidine derivative **4b** for 48 hours at the IC$_{50}$ value. The cells and media supernatants were then washed with ice-cold PBS. The collected cells were then suspended in annexin binding buffer solution (100 mL) "25 mM CaCl$_2$, 1.4 M NaCl, and 0.1 M Hepes/NaOH, pH 7.4" and incubated with "Annexin V-FITC solution (1:100) and propidium iodide (PI)" at a 10 mg mL^{-1} concentration in the dark for 30 min. Stained cells were then acquired using a Cytofex flow cytometer. Then, analysing the cells took place using the flow cytometer BD FACS Calibur (BD Biosciences, San Jose, CA.[72]

3.2.4. Gene expression analysis using RT-PCR. The gene expression of "P53, Bax, caspases-3, 8, 9 as pro-apoptotic genes, and Bcl-2" as the antiapoptotic gene" was assessed to investigate the apoptotic pathway. HCT-116 cells were treated with the pyrimidine derivative **4b** at its IC$_{50}$ value for 48 h. After completing the treatment period, cells were collected, and total RNA was extracted, cDNA was synthesized, a routine RT-PCR reaction, and calculations were performed.[73]

3.3. Molecular docking study

After the EGFR protein (PDB = 1M17) and the chemical structures of compounds were optimised using Maestro, the binding sites within the proteins were identified by utilising grid-box dimensions surrounding the co-crystallized ligands. Next, the AutoDock Vina software was used to dock the examined compounds against the EGFR protein structures, following the

standard procedure. The results of molecular docking are interpreted by binding activities according to binding energy and ligand-receptor interactions. Chimaera was subsequently used for the visualisation. ADME Physicochemical and pharmacokinetic properties were studied using "Molsoft, Molinspiration 2018.10, and SwissADME" web-based software.[74]

4. Conclusion

New pyrimidine-based pyrene, naphtho[1,2-*g*][1,3,5]oxadiazocine, and benzo[5,6]chromeno[4,3-*d*]pyrimidine derivatives were synthesized and fully characterized using multiple spectroscopic techniques. Upon examining their biological activities, hybrid structures **4b,c**, containing bioactive pyrene, pyrimidine, and pyridine moieties, showed potent anticancer activity against HCT-116 cancer cells. Compound **4b** exhibited the most potent inhibitory activity against HCT-116 cancer cells with an IC_{50} value of 1.34 µM, compared to Erlotinib with an IC_{50} value of 1.32 µM. Regarding the EGFR inhibition, compound **4b** exhibited an IC_{50} value of 77.03 nM, compared to Erlotinib (IC_{50} = 72.3 nM). Compound **4b** treatment induced apoptosis in HCT-116 cancer cells by 30.2-fold, halting the cell cycle at the G1-phase. It affected the apoptosis-related genes using the RT-PCR.

Author contributions

Yassin Adam A. Mohammed: writing – original draft, methodology, formal analysis. Ashraf A. Abbas: writing – review & editing, formal analysis, data curation, conceptualization, supervision, project administration. Mohamed S. Nafie: writing the original draft of the biology part, formal analysis, data curation, designing and methodology of all biology parts, and software. Kamal M. Dawood: writing – review & editing, formal analysis, data curation, conceptualization, supervision, project administration. Nabila A. Kheder: writing – review & editing, formal analysis, data curation, conceptualization, supervision, project administration. All authors have read and agreed to the published version of the manuscript.

Conflicts of interest

The authors declare no conflict of interest.

Data availability

The data that support the findings of this study are available on request from the corresponding author

Spectroscopic characterizations and HPLC chromatogram of the synthesized compounds are provided as supporting information. See DOI: https://doi.org/10.1039/d5ra03611a.

References

1 F. Bray, M. Laversanne, H. Sung, J. Ferlay, R. L. Siegel, I. Soerjomataram and A. Jemal, *Ca-Cancer J. Clin.*, 2024, **74**, 229–263.

2 J. Zugazagoitia, C. Guedes, S. Ponce, I. Ferrer, S. Molina-Pinelo and L. Paz-Ares, *Clin. Ther.*, 2016, **38**, 1551–1566.

3 A. Kamal, G. Ramesh, O. Srinivas and P. Ramulu, *Bioorg. Med. Chem. Lett.*, 2004, **14**, 471–474.

4 B. K. Banik and F. F. Becker, *Bioorg. Med. Chem.*, 2001, **9**, 593–605.

5 F. F. Becker and B. K. Banik, *Bioorg. Med. Chem. Lett.*, 1998, **8**, 2877–2880.

6 M. Akhtar, I. Arshad, M. A. Ali, M. Ahmad, M. Mohany and S. S. Al-Rejaie, *Microchem. J.*, 2024, **207**, 111963.

7 A. Jose, S. N. Chathangad, R. Sahadevan, A. Binoy, A. Vignesh, S. Sadhukhan and M. Porel, *J. Photochem. Photobiol., A*, 2023, **444**, 114950.

8 G. R. Suman, M. Pandey and A. S. J. Chakravarthy, *Chem. Front.*, 2021, **5**, 1541–1584.

9 H. Wang, G. Liu, S. Dong, J. Xiong, Z. Du and X. U. Cheng, *J. Mater. Chem. B*, 2015, **3**, 7401–7407.

10 B. Babu, T. A. Ali, T. Ochappan, J. Mack, T. Nyokong and M. G. Sethuraman, *Photodiagn. Photodyn. Ther.*, 2021, **33**, 102102.

11 D. Tzimopoulos, I. Sanidas, A. C. Varvogli, A. Czapik, M. Gdaniec, E. Nikolakaki and P. D. Akrivos, *J. Inorg. Biochem.*, 2010, **104**, 423–430.

12 A. Paul, R. A. Khan, G. M. Shaik, J. P. Shaik, D. S. Nesterov, M. F. C. Guedes da Silva and A. J. L. Pombeiro, *New J. Chem.*, 2024, **48**, 2907–2919.

13 C. G. Oliveira, I. R. Canelón, J. P. C. Coverdale, P. I. S. Maia, G. J. Clarkson, V. M. Deflon and P. J. Sadler, *Dalton Trans.*, 2020, **49**, 9595–9604.

14 C. G. Oliveira, I. R. Canelón, M. M. Silva, J. P. C. Coverdale, P. I. S. Maia, A. A. Batista, S. Castelli, A. Desideri, P. J. Sadler and V. M. Deflon, *Dalton Trans.*, 2019, **48**, 16509–16517.

15 A. Vignesh, A. Binoy, L. Thurakkal, N. S. P. Bhuvanesh, S. Sadhukhan and M. Porel, *J. Mol. Struct.*, 2024, **1295**, 136693.

16 V. N. V. Palakkeezhillam, J. Haribabu, V. S. Kumar, J. F. Santibanez, V. Manakkadan, P. Rasin, M. Garg, N. Bhuvanesh and A. Sreekanth, *Organometallics*, 2024, **43**(3), 242–260.

17 J.-H. Qin, Z. Xiao, J.-R. Zhang, S.-X. Ren, Y.-X. Hu, X.-G. Yang, L.-F. Ma and D.-S. Li, *Dyes Pigm.*, 2022, **205**, 110506.

18 F. P. Kinik, A. Ortega-Guerrero, D. Ongari, C. P. Ireland and B. Smit, *Chem. Soc. Rev.*, 2021, **50**, 3143–3177.

19 A. Gladysiak, T. N. Nguyen, R. Bounds, A. Zacharia, G. Itskos and J. A. Reimer, *Chem. Sci.*, 2019, **10**, 6140–6148.

20 D. Bandyopadhyay, J. L. Sanchez, A. M. Guerrero, F.-M. Chang, J. C. Granados, J. D. Short and B. K. Banik, *Eur. J. Med. Chem.*, 2015, **89**, 851–862.

21 B. Tylińska, B. Wiatrak, Z. Czyżnikowska, A. Cieśla-Niechwiadowicz, E. Gebarowska and A. Janicka-Kłos, *Int. J. Mol. Sci.*, 2021, **22**, 3825.

22 Y. A. A. Mohammed, A. A. Abbas, A. M. Fahim, M. S. Nafie, K. M. Dawood and N. A. Kheder, *J. Mol. Struct.*, 2025, **1347**, 143269.

23 J. Ristovski, R. Minorics, S. Bartha, N. Jankovic and I. Zupkób, *J. Mol. Struct.*, 2022, **1254**, 132373.

24 N. A. Kheder, A. M. Fahim, N. S. Mahmoud and K. M. Dawood, *J. Mol. Struct.*, 2024, **1295**, 136772.

25 N. A. Kheder, A. M. Fahim, N. S. Mahmoud and K. M. Dawood, *J. Mol. Struct.*, 2025, **1330**, 141480.

26 E. Milović, J. Petronijević, N. Joksimović, M. Beljkaš, D. Ružić, K. Nikolić, M. Vraneš, A. Tot, M. Đ. Crnogorac, T. Stanojković and N. Janković, *J. Mol. Struct.*, 2022, **1257**, 132621.

27 O. Afzal, M. Yusuf, M. J. Ahsan, A. S. Altamimi, M. A. Bakht, A. Ali and Salahuddin, *Plants*, 2022, **11**, 2737.

28 P. Seboletswe, P. Awolade and P. Singh, *Chem. Med. Chem.*, 2021, **16**, 2050–2067.

29 Y. Liu, J. Liu, R. Zhang, Y. Guo, H. Wang, Q. Meng, Y. Sun and Z. Liu, *Molecules*, 2019, **24**, 891.

30 H. Mahdy, H. Elnagar and H. Sakr, *J. Pharm. Sci.*, 2023, **67**, 51–67.

31 S. S. Gunathilake, H. D. Magurudeniya, P. Huang, H. Nguyen, E. A. Rainbolt, M. C. Stefan and M. C. Biewer, *Polym. Chem.*, 2013, **4**, 5216–5219.

32 S. Achelle, L. Bodiou, J. Charrier and F. Robin-le Guen, *C. R. Chim.*, 2016, **19**, 279–285.

33 H. D. Trivedi, B. Y. Patel, P. K. Patel and S. R. Sagar, *Russ. J. Org. Chem.*, 2023, **59**, 1769–1782.

34 Z. Dong, J. Wu, X. Shen, Z. Hua and G. Liu, *Chem. Sci.*, 2023, **14**, 3938–3948.

35 R. H. Abd El-Hameed, M. S. Mohamed, S. M. Awad, B. B. Hassan, M. A. E. F. Khodair and Y. E. Mansour, *J. Enzyme Inhib. Med. Chem.*, 2023, **38**, 405–422.

36 H. E. A. Ahmed, M. A. A. El-Nassag, A. H. Hassan, R. M. Okasha, S. Ihmaid, A. M. Fouda, T. H. Afifi, A. Aljuhani and A. M. El-Agrody, *J. Enzyme Inhib. Med. Chem.*, 2018, **33**, 1074–1088.

37 L. M. Al-Harbi, E. A. Harbi, R. M. Okasha, R. A. El-Eisawy, M. A. A. El-Nassag, H. M. Mohamed, A. M. Fouda, A. A. Elhenawy, A. Mora, A. M. El-Agrody and H. K. A. El-Mawgoud, *J. Enzyme Inhib. Med. Chem.*, 2023, **38**, 2155814.

38 H. M. Mohamed, A. M. Fouda, E. S. Khattab, A. M. El-Agrody and T. H. Afifi, *Z. Naturforsch. C*, 2017, **72**, 161–171.

39 S. Gorle, S. Maddila, S. N. Maddila, K. Naicker, M. Singh, P. Singh and S. B. Jonnalagadda, *Anticancer Agents Med. Chem.*, 2017, **17**, 464–470.

40 I. Khan, M. A. Shareef and C. G. Kumar, *Eur. J. Med. Chem.*, 2019, **178**, 1–12.

41 S. R. Abd El Hadi, M. A. Eldinary, A. Ghith, H. Haffez, A. Salman and G. A. Sayed, *RSC Med. Chem.*, 2025, **16**, 2532–2561.

42 D. J. Baillache and A. Unciti-Broceta, *RSC Med. Chem.*, 2020, **11**, 1112–1135.

43 A. Ahmedova, R. Mihaylova, S. Stoykova, V. Mihaylova, N. Burdzhiev, V. Elincheva, G. Momekov and D. Momekova, *Pharmaceutics*, 2023, **15**, 2310.

44 K. M. Dawood, M. A. Raslan, A. A. Abbas, B. E. Mohamed, M. H. Abdellattif, M. S. Nafie and M. K. Hassan, *Front. Chem.*, 2021, **9**, 694870.

45 F. M. Thabet, K. M. Dawood, E. A. Ragab, M. S. Nafie and A. A. Abbas, *RSC Adv.*, 2022, **12**, 23644–23660.

46 K. M. Dawood, M. A. Raslan, A. A. Abbas, B. E. Mohamed and M. S. Nafie, *Anticancer Agents Med. Chem.*, 2023, **23**, 328–345.

47 A. A. Abbas and K. M. Dawood, *Expert Opin. Drug Discovery*, 2022, **17**, 1357–1376.

48 M. E. Salem, E. M. Mahrous, E. A. Ragab, M. S. Nafie and K. M. Dawood, *BMC Chem.*, 2023, **17**, 51.

49 M. E. Salem, E. M. Mahrous, E. A. Ragab, M. S. Nafie and K. M. Dawood, *ACS Omega*, 2023, **8**, 35359–35369.

50 A. A. Abbas and K. M. Dawood, *RSC Adv.*, 2023, **13**, 11096–11120.

51 A. A. Abbas, T. Farghaly and K. M. Dawood, *RSC Adv.*, 2024, **14**, 19752–19779.

52 M. S. Nafie, S. H. Kahwash, M. M. Youssef and K. M. Dawood, *Arch. Pharm.*, 2024, **357**, 2400225.

53 D. M. Mohamed, N. A. Kheder, M. Sharaky, M. S. Nafie, K. M. Dawood and A. A. Abbas, *RSC Adv.*, 2024, **14**, 24992–25006.

54 A. A. Abbas, T. Farghaly and K. M. Dawood, *RSC Adv.*, 2024, **14**, 33864–33905.

55 A. Bin Muhsinah, N. A. Kheder, S. M. Soliman, H. A. Ghabbour, I. A. Elhaty, N. H. Gad and Y. N. Mabkhot, *J. Mol. Struct.*, 2025, **1331**, 141663.

56 M. S. Nafie, S. A. Fahmy, S. H. Kahwash, M. K. Diab, K. M. Dawood and A. A. Abbas, *RSC Adv.*, 2025, **15**, 5597–5638.

57 S. A. Darwish, A. A. Abbas, I. E. El-Sayed, A. M. A. Homoda and K. M. Dawood, *J. Heterocycl. Chem.*, 2025, DOI: 10.1002/jhet.70031.

58 R. B. Bakr and N. A. Elkanzi, *J. Heterocycl. Chem.*, 2020, **57**, 2977–2989.

59 B. Osmiałowski, E. Kolehmainen, R. Dobosz, R. Gawinecki, R. Kauppinen, A. Valkonen, J. Koivukorpi and K. Rissanen, *J. Phys. Chem. A*, 2010, **114**, 10421–10426.

60 T. Mosmann, *J. Immunol. Methods*, 1983, **65**, 55–63.

61 S. M. El Rayes, G. El Enany, I. A. I. Ali, W. Ibrahim and M. S. Nafie, *ACS Omega*, 2022, **7**, 26800–26811.

62 U. Soumyanarayanan, V. G. Bhat, S. S. Kar and J. A. Mathew, *Org. Med. Chem. Lett.*, 2012, **2**, 23.

63 V. P. De Souza, F. S. Santos, F. S. Rodembusch, C. B. Braga, C. Ornelas, R. A. Pilli and D. Russowsky, *New J. Chem.*, 2020, **44**, 12440.

64 M. F. El-Behairy, W. H. Abd-Allah, M. M. Khalifa, M. S. Nafie, M. A. Saleh, M. S. Abdel-Maksoud, T. Al-Warhi, W. M. Eldehna and A. A. Al-Karmalawy, *J. Enzyme Inhib. Med. Chem.*, 2023, **38**, 2157825.

65 I. Shawish, A. Barakat, A. Aldalbahi, W. Alshaer, F. Daoud, D. A. Alqudah, M. Al Zoubi, M. M. Hatmal, M. S. Nafie, M. Haukka, A. Sharma, B. G. de la Torre, F. Albericio and A. El-Faham, *Pharmaceutics*, 2022, **14**, 1558.

66 Z. Kilic-Kurt, N. Ozmen and F. Bakar-Ates, *Bioorg. Chem.*, 2020, **101**, 104028.

67 R. H. Abd El-Hameed, M. S. Mohamed, S. M. Awad, B. B. Hassan, M. A. E. F. Khodair and Y. E. Mansour, *J. Enzyme Inhib. Med. Chem.*, 2023, **38**, 405–422.

68 A. Malki, H. M. Ashour, R. Y. Elbayaa, D. A. Issa, H. A. Aziz and X. Chen, *J. Enzyme Inhib. Med. Chem.*, 2016, **31**, 1286–1299.

69 Z. Kilic-Kurt, Y. Aka and O. Kutuk, *Chem.-Biol. Interact.*, 2020, **330**, 109236.

70 A. M. Gamal-Eldeen, N. A. Hamdy, H. A. Abdel-Aziz, E. A. El-Hussieny and I. M. Fakhr, *Eur. J. Med. Chem.*, 2014, **77**, 323–333.

71 M. López-Gómez, M. Merino and E. Casado, *Clin. Med. Insights: Oncol.*, 2012, **6**, 125–135.

72 I. Lakshmanan and S. K. Batra, *Bio-Protoc.*, 2013, **3**, e374.

73 S. Mocellin, C. R. Rossi, P. Pilati, D. Nitti and F. M. Marincola, *Trends Mol. Med.*, 2003, **9**, 189–195.

74 E. Youssef, M. A. El-Moneim, W. Fathalla and M. S. Nafie, *J. Iran. Chem. Soc.*, 2020, **17**, 2515–2532.

© 2025 The Author(s). Published by the Royal Society of Chemistry